Nuclear Instruments and Methods in Physics Research B 268 (2010) 320–324

Contents lists available at ScienceDirect

Nuclear Instruments and Methods in Physics Research B

journal homepage: www.elsevier.com/locate/nimb

Submicron beam X-ray diffraction of nanoheteroepitaxily grown GaN: Experimental challenges and calibration procedures

P.L. Bonanno [a,*], S. Gautier [b], A.A. Sirenko [c], A. Kazimirov [d], Z.-H. Cai [e], W.H. Goh [a], J. Martin [b], A. Martinez [f], T. Moudakir [b], N. Maloufi [g], M.B. Assouar [h], A. Ramdane [f], L. Le Gratiet [f], A. Ougazzaden [a]

[a] Georgia Institute of Technology/GTL, UMI 2958 Georgia Tech-CNRS, 57070 Metz, France
[b] Laboratoire Matériaux Optiques, Photonique et Micro–Nano Systèmes, UMR CNRS 7132, Université de Metz et SUPELEC, 2 rue E. Belin, 57070 Metz, France
[c] Department of Physics, New Jersey Institute of Technology, Newark, NJ 07102, USA
[d] Cornell High Energy Synchrotron Source (CHESS), Cornell University, Ithaca, New York 14853, USA
[e] Advanced Photon Source, 9700 S. Cass Avenue, Argonne, IL 60439, USA
[f] Laboratoire de Photonique et de Nanostructures, UPR CNRS 20, Route de Nozay, 91460 Marcoussis, France
[g] Laboratoire d'Etude des Textures et Application aux Matériaux, UMR CNRS 7078, Ile du Saulcy, 57045 Metz Cédex 1, France
[h] Laboratoire de Physique des Milieux Ionisés et Applications, Nancy University, CNRS, BP 239, F-54506 Vandoeuvre-lès-Nancy Cédex, France

ARTICLE INFO

Article history:
Received 24 June 2009
Received in revised form 28 August 2009
Available online 18 September 2009

Keywords:
GaN
X-ray diffraction
Synchrotron
Mismatched
Nano
RSM

ABSTRACT

Highly relaxed GaN nanodots and submicron ridges have been selectively grown in the NSAG regime using MOVPE on lattice mismatched 6H–SiC and AlN substrates. 2D real space and 3D reciprocal space mapping was performed with a CCD detector using 10.4 keV synchrotron X-ray radiation at the 2-ID-D micro-diffraction beamline at Advanced Photon Source (APS). Calibration procedures have been developed to overcome the unique challenges of analyzing NSAG structures grown on highly mismatched substrates. We studied crystallographic planar bending on the submicron scale and found its correlation with strain relaxation in the NSAG ridges.

1. Introduction

Progress in nanotechnology depends on adequate characterization tools, such as synchrotron radiation high resolution submicron beam X-ray diffraction [1–4], which is highly sensitive to discerning differences in strain and structural parameters [5]. There is currently a drive to grow group III-nitride nanostructures on highly mismatched substrates [6]. Nondestructive characterization of these structures, while important, and has thus far remained a challenge.

Traditionally, nanostructures are characterized *en masse*, by illuminating a collection of structures and analyzing the diffracted intensity. Sharp peaks strongly suggest uniformity in crystal structure within each nanostructure and across the array. Any broadening in the peaks indicates non-uniformity, though it is impossible to decouple non-uniformity within each structure from inhomogeneity across the group without making often bold assumptions about the symmetries of the structures [7]. However, many of these assumptions are not justified due to complex strain gradients arising from equilibrium between surface and elastic energy in the case of nitride growth [8,9].

Recently, individual micron-scale structures have been measured by high resolution submicron beam X-ray diffraction [2,3]. To isolate individual structures, fluorescence excited by synchrotron beam is first used to map the concentration of elements which exist in the structures of interest. Fluorescence mapping easily discerns high concentrations which correspond to microstructures, even if the substrate is comprised of the same material. However, as we will discuss below, this approach is not always applicable to nano-selective-area grown (NSAG) structures.

Measurement and calibration procedures for overcoming the unique challenges inherent to X-ray diffraction analysis of NSAG dots and ridges on mismatched substrates are the prime focus of this paper. This approach allowed us to locate the NSAG structures in the field, eliminate misalignment between the nanostructure position and the axis of rotation for the θ arm of the goniometer, accurately calculate strain in the regime of lattice mismatched substrates, and correct for misalignment of the charged coupled device (CCD) detector plane with the goniometer sphere.

* Corresponding author. Tel.: +33 3 87 20 39 23; fax: +33 3 87 20 39 40.
E-mail address: PeterBonanno@gatech.edu (P.L. Bonanno).

0168-583X/$ - see front matter © 2009 Elsevier B.V. All rights reserved.
doi:10.1016/j.nimb.2009.09.016

2. Samples

Our samples are comprised of GaN nanodots and submicron ridges nano-selectively grown using metal organic vapor phase epitaxy (MOVPE) on the (0 0 0 1) surfaces of 6H–SiC (samples #1 and #2) and AlN-on-sapphire (sample #3) substrates using an array of 100 nm circular apertures and $120 \times 7600\ nm^2$ stripe-shaped openings etched into the 140 nm thick, $10 \times 10\ \mu m^2$ SiO_2 masks. The samples were grown in a MOVPE T-shaped reactor [10] at 1000 °C using trimethylgallium and ammonia as gallium and nitrogen sources, respectively. Samples #1 and #3 were grown with a pressure of 450 Torr, and sample #2 was grown with a pressure of 100 Torr. More details on the sample growth process can be found in Ref. [11], and sample properties are summarized in Table 1.

3. Challenges

Before one can characterize NSAG structures, one must locate them on the macroscopic-scale substrate. Because achieving selectivity of group III-nitrides requires using tiny mask regions, there is always a rough quality "field" of layer material grown directly on the bare substrate. Finding a $10 \times 10\ \mu m^2$ region of NSAG structures is not trivial, especially when the roughness of the field is on this same length scale.

When the structures of interest are very small (and the spatial resolution requirements very high), slight misalignment between the sample surface and axis of θ rotation cannot be ignored. If the misalignment is not properly corrected, the focused beam footprint will wander across the sample surface during rocking curve measurements.

There is also the matter of calculating strain of the nanostructures without a nearby fully relaxed reference signal. Because the SiC and/or AlN substrates are highly mismatched with respect to GaN nanostructures, one cannot simply scan a small 2θ range around the layer signal and calibrate strain to the nearby substrate signal. For example, when using a 10 keV light source, the nearest sapphire-originating signal is over 10° away in 2θ from the (0 0 .4) signal of fully relaxed GaN. Slight misalignment between the goniometer and actual reciprocal space axes can be ignored for lattice-matched growth, but becomes quite significant for angular ranges of this scale, especially for the q_x direction in reciprocal space.

A CCD detector is the only feasible way to perform 3D reciprocal space mapping (RSM) in any reasonable amount of time, and mapping CCD pixels to angles relative to those reported by the goniometer on which the detector is mounted is complicated by misalignment between the CCD detector and the goniometer sphere. To correct for this, one must determine the full geometry of the misalignment and apply the appropriate transformations to the experimental data.

4. Setup

2D real space and 3D reciprocal space mapping was performed using 10.4 keV synchrotron X-ray radiation at the 2-ID-D beamline of Argonne Photon Source. The beam was focused using a zone plate to a ~240 nm spot with 180 arc sec divergence. Note that there is always a trade off between angular resolution (divergence) of the beam and real space resolution (spot size on the sample surface). Our beam position on the nanostructures was controlled by monitoring Ga–K fluorescence, which was emitted by the GaN nanostructures. An *XYZ* sample stage enabled lateral sample positioning with 50 nm precision. Diffracted intensity was collected by a CCD detector, whose pixel positions were mapped to χ and 2θ diffraction angle values using the substrate and straight beam signals as references for calibration. A CCD detector with inter-pixel distance corresponding to ~8 arc sec was mounted on the goniometer and used to collect diffracted photons. Reciprocal space coordinates were calculated relative to the theoretical values of the bulk GaN [12]. We chose to measure the (0 0 .4) reflection of GaN nanostructures because it provided a strong signal with a reasonably small beam footprint, which varies with $r/\sin\theta_B$, where r is the beam size of 240 nm and θ_B is the Bragg angle for a particular diffraction order. This setup affords a strain accuracy of ±0.0003. A fluorescence detector was positioned near the sample. The setup is shown in Fig. 1.

The positions of the $10 \times 10\ \mu m^2$ masks surrounding the NSAG structures were indicated on the substrate surface by a system of Fe markers. Fe was deposited in a crosshair pattern in the field part of the wafer. This pattern provided an easy way to cross-reference the *XYZ* stage system and the sample coordinate systems by monitoring Fe–*K* fluorescence (6.4 keV) while scanning the sample. Once the Fe markers were mapped, we knew quite precisely where the mask is located, and a fine and tight mapping of Ga–*K* fluorescence in that region quickly revealed the mask position. Mapping this area at the Bragg conditions revealed the profiles of the individual nanostructures (Fig 2c).

5. Correcting for sample-goniometer misalignment

When the NSAG structures, which are located at the sample surface, are not exactly at the axis of rotation for the θ arc, rocking the sample during diffraction measurements will cause the beam footprint to wander the sample surface, often by as much as a few microns, which is greater than the size of the structures being studied. This also creates a situation where the beam footprint is not precisely at the center of the goniometer detector sphere, causing apparent wandering of the diffracted signal in 2θ. This problem of bringing the sample surface to the axis of rotation of the θ arc was solved by adjusting the sample stage elevation (along z direction in Fig. 3) until the local Ga fluorescence profile was constant under sample rocking. Then the precision with which the beam foot print remains stationary on the sample surface for a given rocking measurement is equivalent to the movement of the fluorescence profile caused by rocking the sample over the desired range.

A second source of error is related to imperfect mounting of the sample on the *XYZ* stage. Fig. 3 shows how tilting of the $\langle 0\,0\,.1\rangle$ direction of the sample mounting around the straight beam (y) axis leads to tilting of the true 2θ and χ axes. By knowing the theoret-

Table 1
Growth conditions and measured strain for our samples.

Sample	Substrate	Pressure (Torr)	Field thickness (nm)	Strain (±0.0003)		
				Dots	Ridges	Field
#1	6H–SiC	450	400	−0.0004	−0.0005	−0.0006
#2	6H–SiC	100	400	−0.0011	−0.0012	−0.0015
#3	AlN	450	600	−0.0003	−0.0005	0.0000

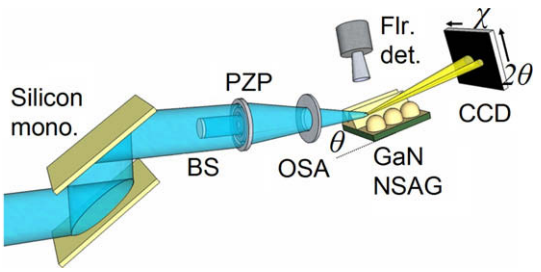

Fig. 1. Experimental setup at the 2-ID-D beamline. Silicon mono., silicon monochromator; BS, gold beam stop; PZP, phase zone plate; OSA, order sorting aperture; GaN NSAG, our sample; Flr. det., fluorescence detector; CCD, CCD detector.

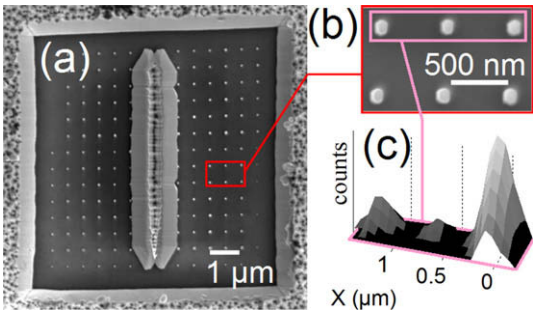

Fig. 2. (a) SEM image of the surface of sample #3, showing the shape and arrangement of the mask and apertures and the NSAG GaN structures grown on top. (b) Higher resolution SEM of selected dots on sample #3. (c) Lateral map of dot region in sample #3 using GaN (0 0 .4) diffraction optimized for the rightmost dot.

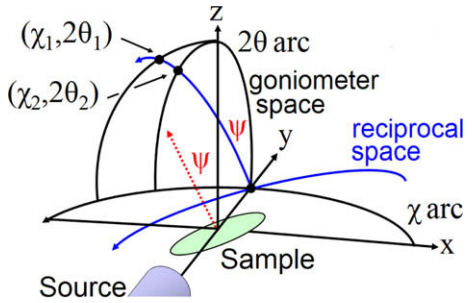

Fig. 3. Qualitative effect of sample tilting around the straight beam axis on actual χ and 2θ arcs in the reciprocal space of the sample (blue) relative to goniometer arcs (black). z direction is the sample stage elevation; y direction is the direction of the straight, undiffracted beam. Tilting of the sample mounting by ψ around the straight beam direction causes the same tilt in reciprocal space relative to the goniometer space. Finding in the goniometer system the position of two reference signals whose theoretical positions in reciprocal space are known allows us to calculate and correct for ψ, determining the reciprocal space. (For interpretation of the references to colour in this figure legend, the reader is referred to the web version of this article.)

ical Bragg conditions of two substrate reflections, $(\chi_{\mathrm{Bragg},1}, 2\theta_{\mathrm{Bragg},1})$ and $(\chi_{\mathrm{Bragg},2}, 2\theta_{\mathrm{Bragg},2})$, and noting the measured positions of these reflections in the goniometer coordinate system, $(\chi_1, 2\theta_1)$ and $(\chi_2, 2\theta_2)$, we can determine the degree of tilting and map the $(\chi, 2\theta)_{\mathrm{gonio}}$ values reported by the goniometer into corresponding actual $(\chi, 2\theta)$ values in the reciprocal space of the sample.

Fig. 3 shows an example in which two symmetric substrate reflections are measured. It can be shown that:

$$\psi = \arcsin\left(\frac{\cos 2\theta_1 \cdot \cos 2\theta_2 \cdot \sin(\chi_1 - \chi_2)}{\sin\left(2\theta_{\mathrm{Bragg},1} - 2\theta_{\mathrm{Bragg},2}\right)}\right), \tag{1}$$

where ψ is the angle between the goniometer and true reciprocal space coordinate systems. Then, the goniometer coordinate system $(\chi, 2\theta)_{\mathrm{gonio}}$ can be mapped to the actual reciprocal space coordinate system by:

$$\begin{pmatrix} \chi \\ 2\theta \\ 1 \end{pmatrix} = R_y(-\psi) \begin{pmatrix} \chi_{\mathrm{gonio}} \\ 2\theta_{\mathrm{gonio}} \\ 1 \end{pmatrix}, \tag{2}$$

where R_y represents a rotation around the y (straight, undiffracted beam) axis in Cartesian space.

6. Mapping a misaligned CCD detector to reciprocal space coordinates

A CCD detector mounted on a goniometer has six degrees of freedom (DOF), three translational and three rotational. Each of these are shown in red[1] in Fig. 4a and b, and are described in the figure caption. All six DOF must be measured and corrected for in order to convert the CCD image into diffraction data. Solving this problem means determining and applying the parameters necessary to map CCD pixel positions (x, y) to $(\Delta\chi, \Delta 2\theta)$ values, which are relative to the $(\chi, 2\theta)$ goniometer readings.

Since these DOF are entirely with respect to the goniometer and not the sample, they can all be deduced using the straight beam, with no sample mounted. We captured multiple CCD images of the straight beam for different goniometer positions along each of the two arcs $2\theta = 0$ and $\chi = 0$, and recorded the pixel position of the straight beam signal on the CCD image for each. Fig. 4a illustrates our CCD pixel coordinate system, with Δx_p and Δy_p directed roughly along the positive $\Delta\chi$ and $\Delta 2\theta$ directions, respectively (the difference being described by the DOF γ). The CCD center, $(\Delta x_p, \Delta y_p) = (\Delta\chi, \Delta 2\theta) = (0, 0)$, comprises two DOF and is defined to be the pixel position of the beam spot at the goniometer position $(2\theta, \chi) = (0, 0)$. Fig. 4a shows the CCD coordinate system and Fig. 4b defines the DOF parameters α, β, γ and L. Descriptions appear in the figure caption.

Fig. 4c shows the geometry for movement along the $\chi = 0$ arc. As we increase the 2θ position of the CCD on the goniometer sphere, the straight beam signal traces out a line in the negative $\Delta 2\theta$ direction. Note that this is not necessarily equal to the Δy_p direction, because of tilting of the CCD detector in γ. Note also that the displacement of this signal from the CCD center along the $\Delta 2\theta$ direction will not necessarily be a linear function of $2\theta_{\mathrm{gonio}}$ because of tilting in α. In fact, it is the deviation from linearity that will determine α.

Let $\Delta y_{2\theta}$ be defined as the offset from $(\Delta x_p, \Delta y_p) = (0, 0)$ along the $\Delta 2\theta$ line, such that $\Delta y_{2\theta}$ and Δy_p have the same sign. For each CCD image along $\chi = 0$, the $\Delta y_{2\theta}$ value of the beam spot was found. Simple geometry reveals that $\Delta y_{2\theta}$ must be a function of L and 2θ: $\Delta y_{2\theta} = -L \sin 2\theta / \cos(2\theta - \alpha)$. By plotting $\Delta y_{2\theta}/\sin 2\theta$ versus 2θ for sufficiently many 2θ positions, we can see the plot $-L/\cos(2\theta - \alpha)$, and L and α can be extracted from the maximum of this plot, which will occur at $(2\theta, \Delta y_{2\theta}/\sin 2\theta) = (\alpha, -L)$ (see Fig. 4d).

An analogous procedure can be used to obtain β. Let Δx_χ be defined like $\Delta y_{2\theta}$, but along the $\Delta\chi$ line and having the same sign as Δx_p. By moving the goniometer through different χ positions on the $2\theta = 0$ arc, and recording Δx_χ for each position, we can plot $\Delta x_\chi/\sin\chi$ and extract β and (redundantly) L from the maximum in the same way as done for α.

To obtain γ, we looked at the CCD images from the $\chi = 0$ arc (used when determining α), and found the angle by which the linear fit of data is tilted with respect to the line $\Delta x_p = 0$. Clearly, $\gamma = \arctan(-\Delta x_p/\Delta y_p)$, where $(\Delta x_p, \Delta y_p)$ is a position of the straight beam signal on any CCD image on this arc.

[1] For interpretation of color in Figs. 3–5, the reader is referred to the web version of this article.

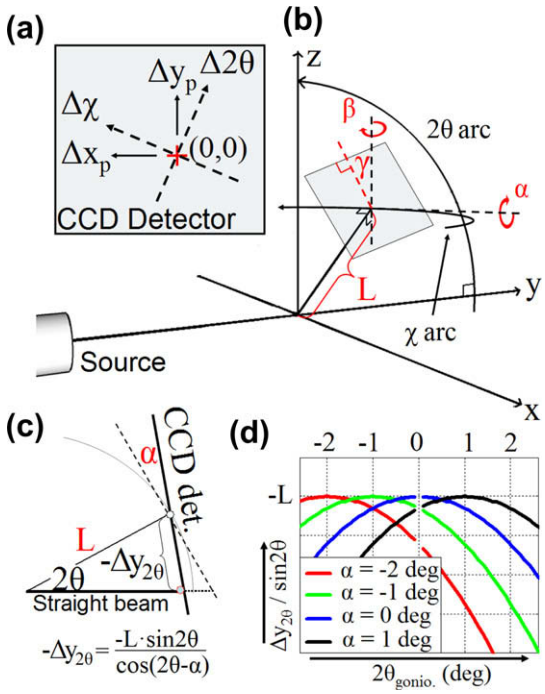

Fig. 4. (a) CCD coordinate system, including origin, pixel axes, and true $(\Delta\chi, \Delta 2\theta)$ axes. Note that positive Δx_p is directed roughly in positive $\Delta\chi$, and not in the usual right-hand Cartesian direction. (b) Three rotational and one translational degrees of freedom of the CCD detector (light grey) with respect to the goniometer arcs. The other two translational degrees are the origin of the CCD detector. L is the distance from the center of the goniometer sphere to the center of the CCD detector. α is the angle between the $\Delta 2\theta$ axis of the CCD detector and the 2θ arc. It is in the clockwise direction around the χ arc. β is the angle between the $\Delta\chi$ axis of the CCD detector and the χ arc. It is in the counterclockwise direction around the 2θ arc. γ is the angle between the Δy_p axis of the CCD detector and the 2θ arc of the goniometer. It is in the counterclockwise direction around the L vector. (c) Geometry of the $\Delta y_{2\theta}$ position of the straight beam signal under motion along the 2θ arc of the goniometer. The dotted line represents the CCD plane for $\alpha = 0$ (perfect alignment). Simple geometry shows that the experimentally determined function $\Delta y_{2\theta}(2\theta) = -L \sin 2\theta/\cos(2\theta - \alpha)$. (d) Plots of $\Delta y_{2\theta}(2\theta)/\sin 2\theta$ for different α values. At the maximum, $\Delta y_{2\theta}/\sin 2\theta = -L$ and $2\theta = \alpha$, determining those two values. (For interpretation of the references to colour in this figure legend, the reader is referred to the web version of this article.)

All DOF of the CCD detector relative to the goniometer sphere are now known. The $(\Delta\chi, \Delta 2\theta)$ value corresponding to any pixel $(\Delta x_p, \Delta y_p)$ can be calculated by:

$$\Delta 2\theta = \arcsin\left(\frac{\Delta y_{2\theta}\cdot\cos\alpha}{\sqrt{L^2+\Delta y_{2\theta}^2+2L\Delta y_{2\theta}\cdot\sin\alpha}}\right)$$
$$\Delta\chi = \arcsin\left(\frac{\Delta x_{\chi}\cdot\cos\beta}{\sqrt{L^2+\Delta x_{\chi}^2+2L\Delta x_{\chi}\cdot\sin\beta}}\right), \quad (3)$$

where

$$\begin{pmatrix}\Delta x_\chi\\ \Delta y_{2\theta}\end{pmatrix} = \begin{pmatrix}\cos(-\gamma) & -\sin(-\gamma)\\ \sin(-\gamma) & \cos(-\gamma)\end{pmatrix}\begin{pmatrix}\Delta x_p\\ \Delta y_p\end{pmatrix}. \quad (4)$$

These offsets are along the goniometer axes and the final goniometer position $(\chi, 2\theta)_{\text{gonio}} + (\Delta\chi, \Delta 2\theta)$, should be transformed to the actual reciprocal space of the sample by Eq. (2).

7. Results

A summary of the results of measurements for our NSAG structures are shown in Table 1. Strain is presented relative to the theoretical values for bulk GaN [12]. We found that all structures are quite relaxed, as expected due to the enormous lattice and thermal mismatch with the SiC or AlN substrates. Differences in strain between structure types on the same sample are smaller than our strain resolution.

By scanning laterally across the ridge structures at the Bragg conditions for the (0 0 .4) reflection of GaN, we noticed a signal which moves in χ depending on lateral position on the ridge. The trend for sample #1 is shown in Fig. 5a, with the corresponding planar arrangement (white) superimposed on the ridges profile (grey). Each continuum of data points corresponds in X to a different facet of the coalesced double-ridge structure, with overlap corresponding to our beam size. Because the χ deviation is so small and we are looking at a symmetric reflection of GaN, we can rule out surface effects and variations in the in-plane lattice parameter a as the source of this signal. Essentially, the tilted planes are creating a secondary reciprocal space system that is tilted by an amount equivalent to the tilting of the planes themselves, in exactly the same way that tilting the entire sample on the stage results in a reciprocal space that is tilted with respect to the goniometer.

Therefore, one can conclude that this secondary signal is due to tilting of the (0 0 .1) planes, which increases in magnitude at a rate of $\Delta\chi/\Delta Z = 0.6°/\mu m$ as one moves away from the center of the each ridge. This is exactly the same rate of tilting observed previously in micro-ridges [2], suggesting that this effect begins in the nano-stages of growth and is typical for both, nano- and microstructures of GaN.

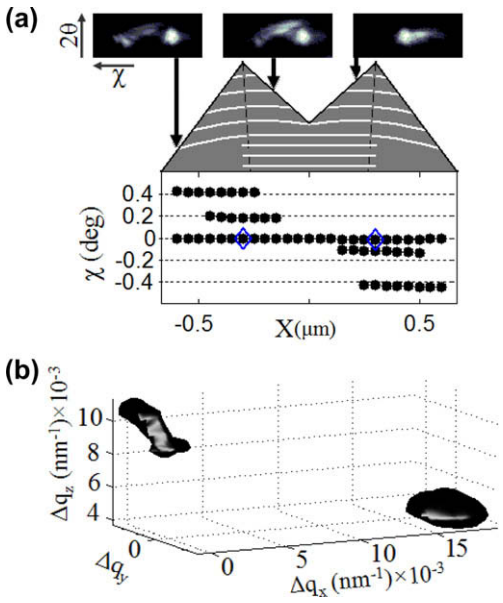

Fig. 5. (a) Diffraction signal distribution for different positions on the coalesced ridge structure for sample #1. Each lateral continuum of $\Delta\chi$ signal originates from one of the four faces, except for the $\Delta\chi = 0$ continuum, which represents untilted planes and has a strong presence for all positions on the ridge structure. The blue diamonds represent the point of peak diffraction and fluorescence intensity corresponding to the ridge apexes. The corresponding planar structure (white) is qualitatively shown on the outline of the ridge structure (grey). The black dotted line qualitatively traces the nucleation site to the ridge apex. (b) 3D diffraction distribution in reciprocal space around the (0 0 .4) reflection of GaN, represented by an iso-intensity surface tracing the intensity at 50% of maximum. This measurement was performed at an extremity of one of the ridges on sample #2, and clearly shows the tilted and untilted signal.

Fig. 5b shows a 3D reciprocal space map around the (0 0 .4) reflection of GaN at an extremity of a ridge on sample #2. Note that there are two signals; one at $q_x = 0$ (untilted) and one at a non-zero (tilted) q_x. Note also that the tilted signal corresponds to less strain than does the untilted signal. Even though this strain difference is within our resolution, the effect is consistently observed for all parts of the nanoridges on all samples, strongly suggesting that the tilting effect is a means by which strain is relieved in nanostructures with smooth free-standing walls. This interpretation is corroborated by our previous results for GaN micro-ridges [2].

In conclusion, by using submicron beam synchrotron X-ray radiation and applying alignment and data calibration techniques, we have overcome the challenges inherent to XRD on NSAG GaN structures grown on highly mismatched substrates. Measurements reveal a clear planar tilting effect in the NSAG ridges, which when combined with 3D RSM, suggest that this tilting effect is a relaxation mechanism for structures with free-standing sidewalls.

Acknowledgements

Use of the Advanced Photon Source at Argonne National Labs was supported by the US Department of Energy, Office of Science, Office of Basic Energy Sciences, under Contract No. W-31-109-ENG-38. Collaboration between GTL and NJIT is supported by the CNRS/USA Collaboration Program UMI 2958. The authors thank Prof. R.D. Dupuis and Dr. J.H. Ryou from Georgia Institute of Technology in Atlanta for providing high quality AlN template substrates for this study.

References

[1] A.A. Sirenko, A. Kazimirov, A. Ougazzaden, S. O'Malley, D.H. Bilderback, Z.-H. Cai, B. Lai, R. Huang, V. Gupta, M. Chien, S.N.G. Chu, Appl. Phys. Lett. 88 (2006) 081111.
[2] P.L. Bonanno, S.M. O'Malley, A.A. Sirenko, A. Kazimirov, Z.-H. Cai, T. Wunderer, P. Brückner, F. Scholz, Appl. Phys. Lett. 92 (2008) 123106.
[3] M. Schmidbauer, P. Schäfer, S. Besedin, D. Grigoriev, R. Köhler, M. Hanke, J. Synchrotron Rad. 15 (2008) 549.
[4] A. Kazimirov, A.A. Sirenko, D.H. Bilderback, Z.-H. Cai, B. Lai, R. Huang, A. Ougazzaden, J. Phys. D: Appl. Phys. 39 (2006) 1422.
[5] J. Stangl, V. Holý, G. Bauer, Rev. Mod. Phys. 76 (2004) 726.
[6] I. Akasaki, J. Cryst. Growth 300 (2007) 2.
[7] M. Schmidbauer, M. Hanke, R. Köhler, Cryst. Res. Technol. 37 (1) (2002) 3.
[8] R.V. Kukta, L.B. Freund, J. Mech. Phys. Solids 45 (11/12) (1997) 1835.
[9] H. Yago, T. Nomura, K. Ishikawa, Appl. Surf. Sci. 84 (1995) 119.
[10] S. Gautier, C. Sartel, S. Ould-Saad, J. Martin, A. Sirenko, A. Ougazzaden, J. Cryst. Growth 298 (2007) 428.
[11] J. Martin, A. Martinez, W.H. Goh, S. Gautier, N. Dupuis, L. Le Gratiet, J. Decobert, A. Ramdane, N. Maloufi, A. Ougazzaden, Mater. Sci. Eng. B, Solid-State Mater. Adv. Technol. 147 (15) (2008) 114.
[12] V. Darakchieva, B. Monemar, A. Usui, Appl. Phys. Lett. 91 (2007) 031911.